Threading dislocations in $La_{0.67}Sr_{0.33}MnO_3/SrTiO_3$ superlattice

Ming He, Long Lin, Hualong Tao, Minghui Qiu, Binyan Zou, Zhihua Zhang

Department of Physics, Liaoning Key Materials Laboratory for Railway, School of Materials Science and Engineering, Dalian Jiaotong University, Dalian 116028, People's Republic of China
E-mail: zhzhang@djtu.edu.cn

Published in Micro & Nano Letters; Received on 29th June 2013; Accepted on 1st August 2013

Transmission electron microscopy-related experiments were performed on a $La_{0.67}Sr_{0.33}MnO_3/SrTiO_3$ superlattice. The predominant defects in the superlattice are a high density of threading dislocations (TDs) perpendicular or quasi-perpendicular to the substrate surface. The TDs are mostly pure-edge-type with Burgers vectors $\boldsymbol{b} = \langle 100 \rangle$ or $\langle 110 \rangle$. A few TDs of screw character with Burgers vectors $\pm[001]$ were also found. Electron energy loss spectra show that non-stoichiometry is accommodated in the near-interface region of the superlattice. The stronger crystal field induced by defect and non-stoichiometry are accounted for by the observed macroscopic properties.

1. Introduction: Studies on superlattices, composed of alternating heteroepitaxial perovskite oxide layers, have increased dramatically because they offer the possibility to control the interlayer coupling between neighbouring ferromagnetic layers [1–3]. Many intriguing physics phenomena, such as anomalous Hall effect, insulator–metal transition, etc. have been observed in this kind of superlattice [1–3]. The superlattices containing many interfaces of interest, the carrier confinement effect, specific magnetic interaction and some lattice strain effect at the interface play an important role on the properties of the superlattices [4]. These physical effects at the interface are closely related to interface microstructures. Some defects, such as stacking faults and threading dislocations (TDs), at the interface thus have an adverse impact on device performance [5]. The detailed studies on the microstructure of the superlattices, especially defects nature, are crucial for understanding system properties and for fabricating high-quality epitaxial layers. So far, many works have been published on the microstructure characterisations of single film grown on substrates [6–8]. However, the studies on microstructures of superlattice are scarce. Transmission electron microscopy (TEM) is an effective way for investigating superlattices with a high spatial resolution, and diffraction contrast images give information on the dislocations and defects during the growth process. This combination of techniques related to TEM allows one to obtain insight into the microstructure of the materials.

The $La_{0.67}Sr_{0.33}MnO_3$(LSMO)/$SrTiO_3$(STO) superlattice is one of the most studied systems. In our previous studies, we have observed oscillatory exchange coupling and enhanced magnetoresistance in such superlattices [9, 10]. The study on the electronic structures evolution across the interface of the superlattice provides a plausible explanation for the observed physical properties, that is, a stronger crystal field and/or a partial loss of oxygen at the interfacial regions [11]. In this reported work, we looked at different aspect of the LSMO/STO superlattices, studied the defects nature and the evolution of defects across multiple interfaces, by analysing details of the cross-sectional bright field TEM micrograph. The epitaxial relationships of the superlattice were revealed by selected-area electron diffraction (SAED) and high-resolution TEM (HRTEM). A high density of TDs had been found in the superlattice, the types and Burgers vectors of these TDs were analysed. No misfit dislocations (MDs) were observed in the superlattice, the microstructure could be related to the macroscopic properties of the same superlattice system in terms of crystal field point.

2. Experiment: The LSMO/STO superlattices were grown on the (001) STO single crystal substrates by pulsed laser deposition (PLD) method, which demonstrates a novel exchange bias effect and enhanced magnetoresistance [9, 10]. Stoichiometric-sintered STO and LSMO ceramic targets were prepared by the conventional solid-state reaction method. An XeCl excimer pulsed laser beam (Lambda Physic Compex205, $\lambda = 308$ nm, $\tau = 28$ ns) was introduced to prepare the LSMO/STO superlattice. A buffer LSMO layer of 60 nm in thickness was deposited prior to the growth of the LSMO/STO superlattices to diminish substrate-induced strain. The LSMO and STO layer were grown on a (001) STO substrate at 780°C in oxygen pressure of 40 Pa. After deposition, the samples were annealed *in situ* at 700°C and in ambient oxygen of 0.8 atm for 2 h to avoid the oxygen deficiency. The cross-sectional TEM specimen was prepared in a standard way, first by cutting, gluing and mechanically polishing, and then the Ar-ion milling instrument was used until perforation occurred. The TEM experiments were performed with a Philips CM200 and a Tecnai F20 transmission electron microscope; both were supertwin field-emission gun TEMs equipped with Gatan imaging filter systems at 200 kV. For bulk materials, $SrTiO_3$ had a cubic cell with lattice parameter $a = 3.905$ Å and $La_{0.67}Sr_{0.33}MnO_3$ had a pseudocubic cell with $a = 3.873$ Å.

3. Results and discussions: Fig. 1*a* shows a cross-sectional bright field TEM micrograph of the studied LSMO/STO superlattice on the (001) STO substrate. The layers can be easily distinguished due to different contrasts; the thicker bands are corresponding to the LSMO layers and the thinner bands to the STO layers. Fig. 1*b* shows a scanning TEM (STEM) image of the studied system. The contrasts are different from the conventional image in Fig. 1*a*: the bright bands are corresponding to the LSMO layers and the dark bands to the STO layers. The film exhibits sharp, flat and well-defined interfaces between successive LSMO and STO layers. The SAED pattern taken from the region containing all the films and substrate is shown in Fig. 1*c*. Details of the 004 beam indicates two different parameters of STO and LSMO in the growth direction. The orientation relationship between epitaxially grown STO and LSMO films are (001) STO//(001) LSMO//(001) $LSMO_{buffer}$//(001) $STO_{substrate}$ and [010] STO//[010] LSMO//[001] $LSMO_{buffer}$//[010] $STO_{substrate}$. The HRTEM image in Fig. 1*d* shows the epitaxy across the interface, with no secondary phase or amorphous layer present along the interface. The modulation period of the superlattice can be estimated as 4 nm for STO layers and 11 nm for LSMO layers.

A study of the many areas in the specimen shows that the predominant defects in the superlattice system are a high density of TDs, being perpendicular or quasi-perpendicular to the substrate surface. Fig. 2*a* shows a typical cross-sectional bright field TEM

doi: 10.1049/mnl.2013.0411

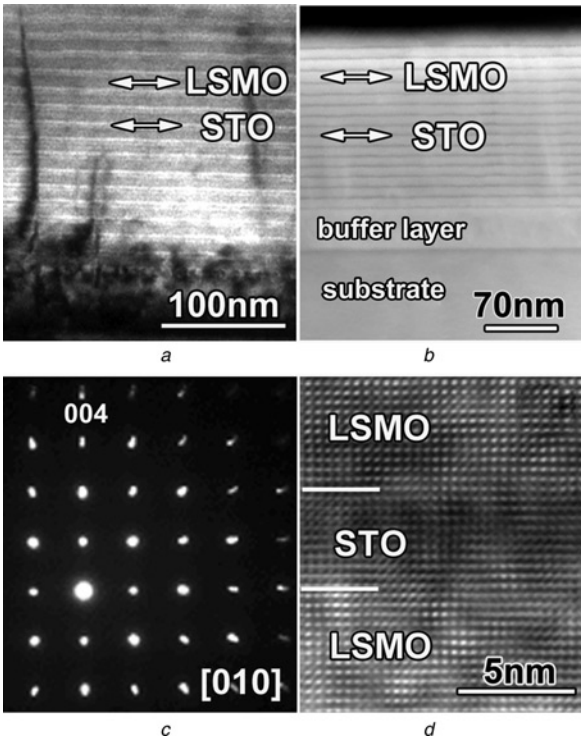

Figure 1 *Microstructure of the studied LSMO/STO superlattice*
a Cross-sectional bright field TEM micrograph
b STEM image
c SAED pattern taken from the superlattice
d HRTEM image

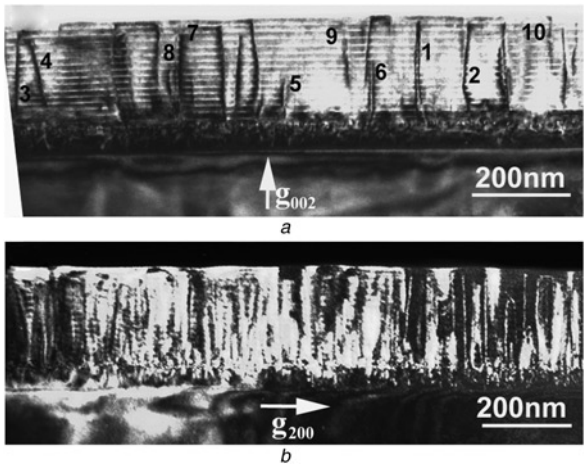

Figure 2 *Cross-sectional bright field TEM micrograph taken with diffraction vector* $\boldsymbol{g} = (002)$ *under near two-beam conditions and WBDF image taken with diffraction vector* $\boldsymbol{g} = (200)$
a TEM micrograph
b WBDF image

micrograph taken with diffraction vector $\boldsymbol{g} = (002)$ under near two-beam conditions, from which the information about the evolutions of typical TDs can be obtained. The dislocations denoted by 1 and 2 originated from the LSMO/STO interface and threaded through many LSMO/STO interfaces to the top of the superlattice. The dislocation lines 3 and 4 were threaded from the first LSMO layer; however, they met each other and formed a half loop after penetrating a few LSMO/STO interfaces. The lines 5 and 6 were also threaded from the LSMO layer, but they stop in the centre of the superlattice after threading several interfaces. Dislocations 7 and 8, as segments of a half loop, originate from the LSMO/STO interface, and terminate in the centre of the superlattice. For dislocations 9 and 10, they originate from the centre of the studied system. Fig. 2*b* shows a weak beam dark field (WBDF) image of the same area, taken with diffraction vector $\boldsymbol{g} = (200)$. Compared with Fig. 2*a*, many more TDs can be seen as bright lines propagating in a direction normal to the substrate surface. Most of these TDs were generated from the STO substrate or the STO/LSMO interfaces and threaded to the superlattice. According to the diffraction contrast theory, it can be concluded that the TDs in Fig. 2*b* primarily have Burgers vectors parallel to the superlattice interface and are edge dislocations, whereas all the visible TDs in Fig. 2*a* have Burgers vectors with screw components normal to the substrate surface ($b = \pm[001]$).

In addition, there are some white dots at the interface between the buffer layer and the first STO layer in both Figs. 2*a* and *b*, which show the contrast of misfit dislocations under the imaging conditions of $\boldsymbol{g} = (002)$ and (200). This indicates that the misfit dislocations are of edge character and Burgers vectors have [100] and [001] components. Although there also exists lattice mismatch of the superlattice, no misfit dislocations are observed in the LSMO/STO interface. This can be explained by critical layer thickness [12], when this thickness is attained, strain relief is supposed to occur by the formation of misfit dislocations. For the case of LSMO and STO layers, the critical thicknesses were calculated as ~18 nm. While considering the case of the whole superlattice grown on LSMO buffer layer, the critical thickness of the whole film was calculated to be about 90 nm. So the actual thicknesses of the individual LSMO and STO layer (11 and 4 nm estimated from the HRTEM and STEM images, respectively) are both smaller than their critical thicknesses, whereas the total thickness of the superlattice is larger than its critical value. Thus, there should be some MDs at the interface between LSMO buffer layer

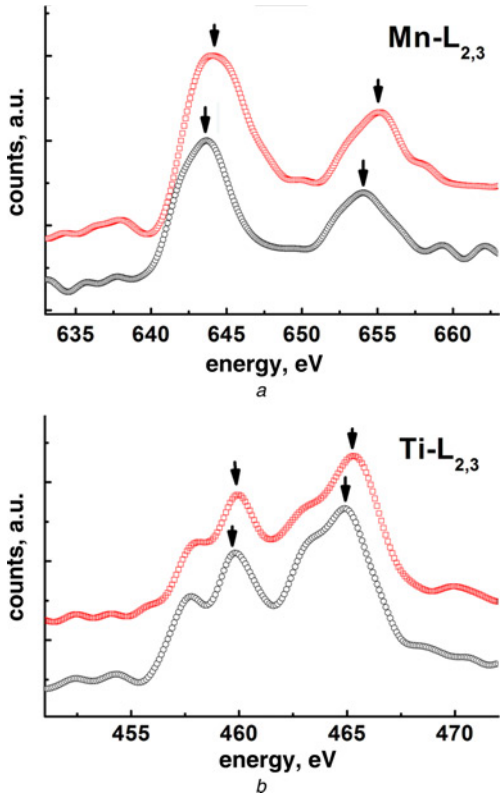

Figure 3 *Energy loss near-edge spectra of*
a Mn-$L_{2,3}$
b Ti-$L_{2,3}$ edges
Upper spectra are taken from the LSMO layer and the lower ones are taken from the LSMO/STO interface

and the supperlattice, whereas there are no MDs in the interfaces between the LSMO/STO layers in the superlattice. Being consistent with the fact that no misfit dislocations, can be seen there would exist strain and a lattice deformation in the interface of the superlattice to match the in-plane lattice constant of the substrate. The dislocation density in the buffer layer LSMO is much higher than that in the subsequent layer, which illustrates the importance of the buffer layer for the growth of a high-quality superlattice.

The types of misfit-induced lattice defects are often related to cation and anion non-stoichiometry [13]. In fact, we indeed observed the non-stoichiometry in the near-interface region. Figs. 3*a* and *b* show the energy loss near-edge spectra of Mn-$L_{2,3}$ and Ti-$L_{2,3}$ edges. The upper spectra in Figs. 3*a* and *b* are taken from the LSMO layer and the lower ones are taken from the LSMO/STO interface. The similar trends of peak shifting are observed for both Mn-$L_{2,3}$ and Ti-$L_{2,3}$ edges when the electron probes move from the LSMO layer to the LSMO/STO interface: the energy positions of Mn-$L_{2,3}$ and Ti-$L_{2,3}$ edges shifted towards lower-energy losses (red-shifted), suggesting a local under-stoichiometry of oxygen around Mn and Ti at the interfacial region [11]. The large lattice mismatch and non-stoichiometry in the near-interface region all contribute to the formation of TDs.

4. Conclusions: The predominant defects in the LSMO/STO superlattice epitaxially grown on the (001) STO substrate by PLD method had a high density of edge-type TDs with $\boldsymbol{b} = \langle 100 \rangle$ or $\langle 110 \rangle$. A few TDs of screw character were also found and the WBDF image revealed the screw components of their Burgers vectors were $\pm[001]$. The TDs were generated near the STO/LSMO interfaces as a result of the non-stoichiometry during the stages of film growth. No misfit dislocations were observed in the superlattice. Because of the presence of defects and departures from stoichiometry, these two factors both lead to the strengthening of the crystal field in the interface region, accounting for the observed macroscopic properties in the studied LSMO/STO superlattice.

5. Acknowledgment: The authors acknowledge that this work was sponsored by the National Natural Science Foundation of China under Grants No. 50902014, 51002017 and 61274063.

References

[1] Wang L. M.: 'Anomalous Hall effect in $La_{0.7}Sr_{0.3}MnO_3/SrTiO_3$ superlattices: hopping transport and a probe of dimensionality', *Phys. Rev. Lett.*, 2006, **96**, (7), pp. 077203–077206

[2] Nikolaev K. R., Dobin A.Yu., Krivorotov I. N., *ET AL.*: 'Oscillatory exchange coupling and positive magnetoresistance in epitaxial oxide heterostructures', *Phys. Rev. Lett.*, 2000, **85**, (17), pp. 3728–3731

[3] Moutis N., Christides C., Panagiotopoulos I., Niarchos D.: 'Exchange-coupling properties of $La_{1-x}Ca_xMnO_3$ ferromagnetic antiferromagnetic multilayers', *Phys. Rev. B*, **64** (9), p. 0944291

[4] Izumi M., Murakami Y., Konishi Y., Mananko T., Kawasaki M., Tokura Y.: 'Structure characterization and magnetic properties of oxide superlattices $La_{0.6}Sr_{0.4}MnO_3/La_{0.6}Sr_{0.4}FeO_3$', *Phys. Rev. B*, 1999, **60**, (2), pp. 1211–1215

[5] Zhao K., Jin K. J., Lu H. B., *ET AL.*: 'Electrical-modulated magnetoresistance in multi-*p*-*n* heterojunctions of $La_{0.9}Sr_{0.1}MnO_3$ and oxygen-vacant $SrTiO_{3-\delta}$ on Si substrates', *Appl. Phys. Lett.*, 2008, **93**, (25), pp. 252110–252112

[6] Lu C. J., Bendersky L. A., Lu H., Schaff W. J.: 'Threading dislocations in epitaxial InN thin films grown on (0001) sapphire with a GaN buffer layer', *Appl. Phys. Lett.*, 2003, **83**, (14), pp. 2817–2819

[7] Kehagias Th., Delimitis A., Komninou Ph., *ET AL.*: 'Misfit accommodation of compact and columnar InN epilayers grown on Ga-face GaN (0001) by molecular-beam epitaxy', *Appl. Phys. Lett.*, 2005, **86**, (15), pp. 151905–191907

[8] Qi X. Y., Miao J., Duan X. F., Zhao B. R.: 'Microstructure of $La_{0.7}Sr_{0.3}MnO_3/Ba_{0.7}Sr_{0.3}TiO_3/La_{0.7}Sr_{0.3}MnO_3$ epitaxial films grown on (0 0 1) $SrTiO_3$ substrate', *J. Crys. Grow.*, 2005, **277**, (1), pp. 218–222

[9] Zhu S. J., Yuan J., Zhu B. Y., *ET AL.*: 'Exchange bias effect and enhanced magnetoresistance in $La_{0.67}Sr_{0.33}MnO_3/SrTiO_3$ superlattices', *Appl. Phys. Lett.*, 2007, **90**, (11), pp. 112502–112504

[10] Zhu S. J., Zhao B. R., Zhu B., Xu B., Cao L. X., Qiu X. G.: 'Oscillatory exchange coupling in $La_{0.67}Sr_{0.33}MnO_3/SrTiO_3$ superlattices', *Appl. Phys. Lett.*, 2007, **91**, (1), pp. 012505–012507

[11] He M., Zhang Z. H.: 'Interface structures of $La_{0.67}Sr_{0.33}MnO_3/SrTiO_3$ superlattices studied by TEM and EELS', *J. Phys. Chem. C.*, 2010, **114**, (30), pp. 13068–13070

[12] People R., Beam J. C.: 'Calculation of critical layer thickness versus lattice mismatch for Ge_xSi_{1-x}/Si strained–layer heterostructures', *Appl. Phys. Lett.*, 1985, **47**, (3), pp. 322–324

[13] Suzuki T., Nishi Y., Fujimoto M.: 'Effect of nonstoichiometry on microstructure of epitaxially grown $BaTiO_3$ thin films', *Jpn. J. Appl. Phys.* 2000, **39**, (10), pp. 5970–5976

doi: 10.1049/mnl.2013.0411